ARTICLES
PUBLISHED ONLINE: 23 NOVEMBER 2008 | DOI: 10.1038/NMAT2329
nature materials

Thermally stable Pt/mesoporous silica core–shell nanocatalysts for high-temperature reactions

Sang Hoon Joo, Jeong Young Park, Chia-Kuang Tsung, Yusuke Yamada, Peidong Yang and Gabor A. Somorjai*

Recent advances in colloidal synthesis enabled the precise control of the size, shape and composition of catalytic metal nanoparticles, enabling their use as model catalysts for systematic investigations of the atomic-scale properties affecting catalytic activity and selectivity. The organic capping agents stabilizing colloidal nanoparticles, however, often limit their application in high-temperature catalytic reactions. Here, we report the design of a high-temperature-stable model catalytic system that consists of a Pt metal core coated with a mesoporous silica shell ($Pt@mSiO_2$). Inorganic silica shells encaged the Pt cores up to 750 °C in air and the mesopores providing direct access to the Pt core made the $Pt@mSiO_2$ nanoparticles as catalytically active as bare Pt metal for ethylene hydrogenation and CO oxidation. The high thermal stability of $Pt@mSiO_2$ nanoparticles enabled high-temperature CO oxidation studies, including ignition behaviour, which was not possible for bare Pt nanoparticles because of their deformation or aggregation. The results suggest that the $Pt@mSiO_2$ nanoparticles are excellent nanocatalytic systems for high-temperature catalytic reactions or surface chemical processes, and the design concept used in the $Pt@mSiO_2$ core–shell catalyst can be extended to other metal/metal oxide compositions.

To design high-performance catalysts in terms of activity, selectivity and resistance to deactivation, understanding the properties affecting catalytic performance is of great importance[1–4]. Over the past few decades, model catalytic systems, including metal single crystals and lithographically fabricated metal nanostructures, have successfully been used to uncover atomic-scale characteristics, such as surface structures and particle size, that are critical to catalytic activity and selectivity[5–8]. Recent advances in colloid chemistry enabled catalytic nanoparticles to be readily prepared with tunable particle size, shape and composition[9–13]. Starting with colloidal nanoparticles, two-dimensional (2D) and 3D model catalysts have been developed that are composed of arrays of nanoparticles on a flat substrate and nanoparticles dispersed on a high-surface-area mesoporous oxide support, respectively. These model catalytic systems have enabled systematic investigations of the effects of particle size[14], shape[15–17] and composition[18,19] on catalytic properties.

Catalytic studies of colloidal nanoparticles have shown that the thermal and chemical stabilities of nanoparticle catalysts are crucial. Colloidal nanoparticles are usually prepared in the presence of organic capping agents, such as polymers or surfactants, that prevent the aggregation of nanoparticles in solution. At high temperatures, typically above 300 °C, however, the organic capping layers can decompose and the metal nanoparticles can deform and aggregate. As a result, the size, shape and composition of nanoparticles during or after high-temperature reactions could be different from those of pristine nanoparticles. Many industrially important catalytic processes, including CO oxidation[20–25], partial oxidation[26] and cracking[27] of hydrocarbons and combustion[28] reactions, are carried out at temperatures above 300 °C. In this regard, model catalysts that are stable at high reaction temperatures are in high demand.

Here, we designed core–shell particle configurations and prepared the nanoparticles with high thermal stability. The core–shell structures have important implications in catalysis[29]. The outer shells isolate the catalytically active nanoparticle cores and prevent the possibility of sintering of core particles during catalytic reactions at high temperatures. In addition, the synergistic effects of metal–support interfaces may be maximized where such interfaces are important in catalytic performances.

Herein, we report the preparation of Pt/mesoporous silica core–shell ($Pt@mSiO_2$) nanoparticles that are thermally stable at high temperatures. We carried out CO oxidation and ethylene hydrogenation reactions to explore the catalytic activities of the $Pt@mSiO_2$ core–shell nanoparticles. The core–shell structured $Pt@mSiO_2$ nanoparticles were prepared in three steps (Fig. 1): (1) synthesis of Pt nanoparticles using tetradecyltrimethylammonum bromide (TTAB) as the capping agent, (2) silica polymerization around the Pt cores, generating the as-synthesized $Pt@SiO_2$ mesostructures and (3) removal of the TTAB molecules by calcination to produce the $Pt@mSiO_2$ core–shell nanoparticles. The $Pt@mSiO_2$ consisted of 14 nm Pt cores and 17-nm-thick mesoporous silica shells. The reacting molecules can directly access the Pt cores through the mesopores within the silica shells and the product molecules can readily exit through these mesopores. The Pt cores were encaged within the silica shells at temperatures up to 750 °C in air. The $Pt@mSiO_2$ nanoparticle catalysts exhibited catalytic activity similar to TTAB-capped Pt nanoparticles for ethylene hydrogenation and CO oxidation. Significantly, the high thermal stability of $Pt@mSiO_2$ nanoparticles enabled the study of ignition behaviour during the Pt-nanoparticle-catalysed CO oxidation process. The high thermal stability, as well as uniform mesoporous shell structure, suggested that the $Pt@mSiO_2$ core–shell nanoparticles are an excellent nanoparticle system for catalytic reactions or surface chemical processes that occur at high temperatures.

The transmission electron microscope (TEM) images for TTAB-capped Pt and as-synthesized $Pt@SiO_2$ nanoparticles are

Department of Chemistry, University of California and Chemical Sciences and Materials Sciences Divisions, Lawrence Berkeley National Laboratory, Berkeley, California 94720, USA. *e-mail: somorjai@berkeley.edu.

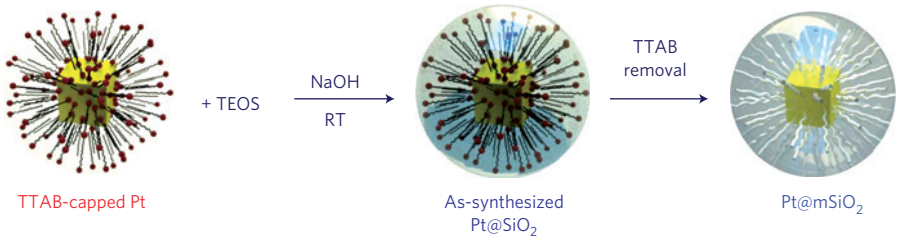

Figure 1 | Schematic representation of the synthesis of Pt@mSiO$_2$ nanoparticles. Pt nanoparticles were synthesized using TTAB surfactant as the capping agent, and used as the core particles. Second, as-synthesized Pt@SiO$_2$ particles were prepared by polymerizing TEOS around the TTAB-capped Pt cores. RT: room temperature. The as-synthesized Pt@SiO$_2$ particles were subsequently converted to Pt@mSiO$_2$ particles by calcination.

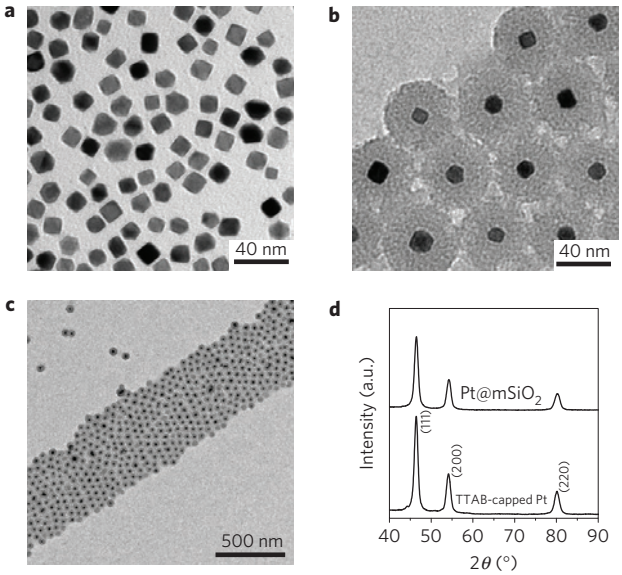

Figure 2 | TEM and XRD characterizations of TTAB-capped Pt and as-synthesized Pt@SiO$_2$ core–shell nanoparticles. a–c, TEM images of TTAB-capped Pt (**a**) and as-synthesized Pt@SiO$_2$ nanoparticles (**b**,**c**). **d**, High-angle XRD patterns of Pt and Pt@SiO$_2$ nanoparticles.

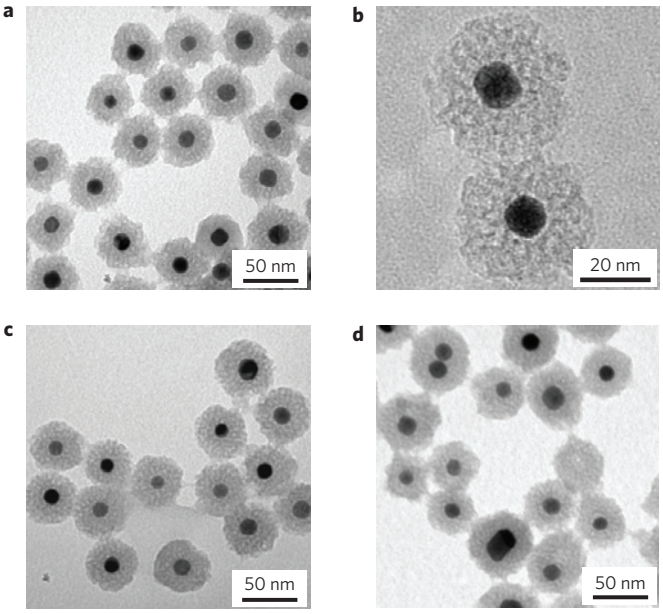

Figure 3 | Thermal stability of Pt@mSiO$_2$ nanoparticles. a–d, TEM images of Pt@mSiO$_2$ nanoparticles after calcination at 350 °C (**a**,**b**), 550 °C (**c**) and 750 °C (**d**).

shown in Fig. 2. The TTAB-capped Pt nanoparticles shown in Fig. 2a were composed of a mixture of cubes (70%), cuboctahedra (26%) and irregular shapes (4%) and exhibited an average particle size around 14.3 nm in diagonal distance. The surfaces of these Pt cubes are stabilized by the bilayer of the TTAB surfactants[30]. These surface-capping TTAB surfactants were also used as structure-directing templates for the polymerization of silicates by a sol–gel process, as demonstrated in the synthesis of MCM-41-like ordered mesoporous silicas[31,32]. The silica–TTAB layer was formed around the Pt nanoparticles under basic conditions (pH = 10–11) through an electrostatic interaction between the cationic (TTAB) and anionic (silicate) species. The TEM images of as-synthesized Pt@SiO$_2$ obtained under optimized experimental conditions (Pt colloid/tetraethylorthosilicate (TEOS) = 1:4.5), where each Pt particle is encapsulated by a silica layer, are shown in Fig. 1. The average thickness of the silica layer surrounding the Pt core was around 17 nm. Figure 2c shows the closely assembled structure of the Pt@SiO$_2$ nanoparticles in a large area, which was formed by drop-casting on a TEM grid. The X-ray diffraction (XRD) patterns of Pt and Pt@SiO$_2$ nanoparticles (Fig. 2d) revealed that the crystal structure (face-centred-cubic) of the TTAB-capped Pt nanoparticles was maintained after the formation of the silica layer on the Pt.

Most (~95%) of the as-synthesized Pt@SiO$_2$ nanoparticles shown in Fig. 2b,c exhibited the core–shell structures, where each Pt particle is encaged within a silica shell. The configuration of core–shell nanoparticles was tuned by changing the concentration of the silica source (TEOS) added for the silica polymerization. If the concentration of TEOS was decreased compared with the amount required for the optimized condition, the silica shell contained multiple Pt particles (see Supplementary Information, Fig. S1a). Increasing the amount of TEOS resulted in the formation of a mixture of Pt@mSiO$_2$ and amorphous silica particles without Pt cores (see Supplementary Information, Fig. S1b). This synthetic strategy can be generally applicable to nanoparticles with differing composition, size and shape. For instance, smaller size 8.5 nm TTAB-capped Pt nanoparticles can be readily converted into Pt@SiO$_2$ core–shell particles, as shown in Supplementary Information, Fig. S2.

The as-synthesized Pt@SiO$_2$ nanoparticles contained a significant amount of the TTAB surfactants, which are unfavourable for molecular diffusion of reactant and product in catalytic applications. To remove the TTAB surfactants, the as-synthesized Pt@SiO$_2$ sample was calcined at 350 °C for 2 h in static air to yield mesoporous Pt@mSiO$_2$ nanoparticles. The TEM images of Pt@mSiO$_2$ nanoparticles after calcination (Fig. 3a,b) exhibited mesopores of 2–3 nm in the silica shells. The porosity of Pt@mSiO$_2$ was confirmed by nitrogen physisorption. The nitrogen adsorption–desorption isotherms of Pt@mSiO$_2$ calcined at 350 °C (Fig. 4a) revealed that these nanoparticles are mesoporous,

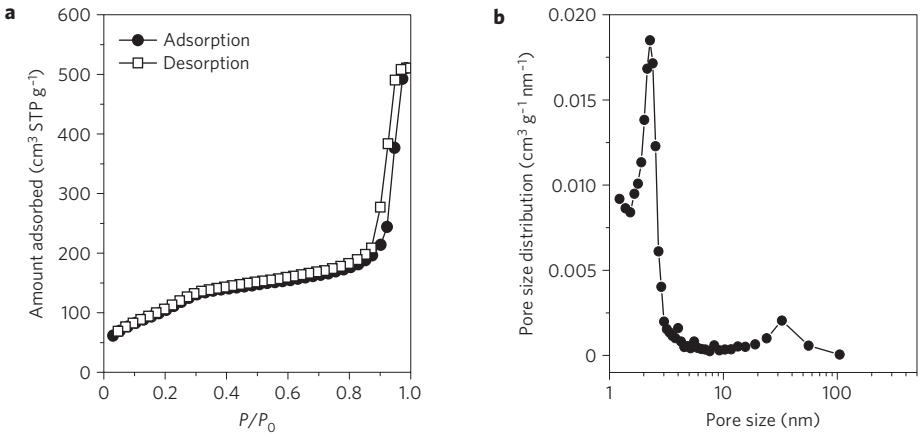

Figure 4 | Structural characterization of Pt@mSiO$_2$ nanoparticles calcined at 350 °C. a, Nitrogen adsorption–desorption isotherms. **b**, Pore size distribution calculated from the adsorption branch of the isotherms.

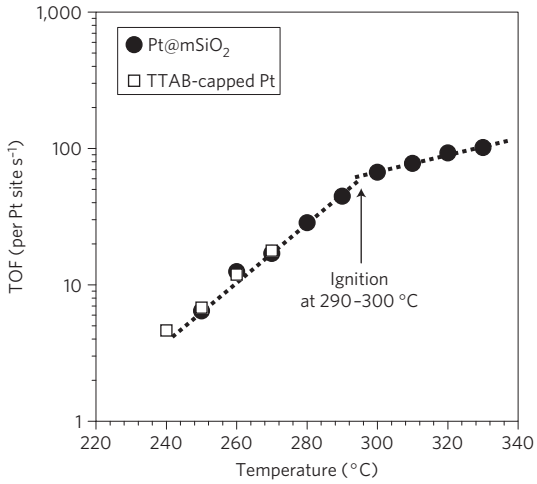

Figure 5 | CO oxidation activity of TTAB-capped Pt and Pt@mSiO$_2$ nanoparticles.

as identified by the increase of the adsorption amount in the relative pressure (P/P_0) range of 0.2–0.3. The pore size distribution curve calculated from the adsorption branch of the isotherms (Fig. 4b) exhibited a maximum at 2.3 nm and the Brunauer–Emmett–Teller surface area of Pt@mSiO$_2$ was calculated to be 440 m^2 g^{-1}, indicating the highly mesoporous nature of the silica shell.

For core–shell nanoparticles to be catalytically active, direct access of reactive molecules to the core particles is of significant importance. In previous examples of metal/mesoporous silica core–shell particles[33–35], an intermediate protecting amorphous silica layer was often sandwiched between the metal core and the mesoporous silica layer, thus hampering direct access of reactants to the metal core. In our design of these core–shell particles, the mesoporous silica layer was directly formed on the Pt cores. The accessibility of gas molecules was directly proved by chemisorption measurements. Hydrogen chemisorption over the Pt@mSiO$_2$ catalyst gave a dispersion value of 8 ± 0.5%, which is comparable to the ratio of surface atoms (11%) on the Pt particle, as calculated by geometric considerations[36].

After calcination at 350 °C, the spherical core–shell shape of the as-synthesized Pt@SiO$_2$ particles was maintained, as can be seen by comparing the TEM images before (Fig. 2b) and after (Fig. 3a) calcination. The shape of the Pt cores inside Pt@mSiO$_2$ became slightly rounder after calcination, which is presumably due to the melting of the Pt particles at the Pt–silica interface, as reported earlier[37]. However, a closer observation of the Pt core by high-resolution TEM (Supplementary Information, Fig. S3) revealed that the Pt core continued to be faceted and single crystalline after thermal treatment under air. The stability of Pt@mSiO$_2$ core–shell nanoparticles at higher temperatures was investigated by heating the sample to 550 °C and 750 °C in air. After the calcination at 550 °C (Fig. 3c), the core–shell morphology of Pt@mSiO$_2$ nanoparticles was preserved. Even on heating the sample as high as 750 °C, the morphology of most Pt@mSiO$_2$ nanoparticles was maintained and the Pt cores were still encaged within the silica shells (Fig. 3d), indicating high thermal stability of Pt@mSiO$_2$ core–shell nanoparticles. It is interesting to note that in the case of the sample calcined at 750 °C, some core–shell particles possessing larger Pt cores and Pt-free hollow silica particles were found. It seemed that Pt cores in Pt@mSiO$_2$ nanoparticles diffused around 750 °C through the mesoporous silica shell into the neighbouring Pt@mSiO$_2$ particles. A detailed study of the thermal evolution of Pt@mSiO$_2$ nanoparticles is now underway.

The noble metal/metal oxide core–shell structured nanoparticles have recently been exploited for catalytic applications[38–43]. Examples include Pt@CoO yolk–shell nanoparticles[38], poly(vinylpyrrolidone)-capped Pt encapsulated in mesoporous silica[39], Pt nanoparticles entrapped in hollow carbon shells[40] and Au nanoparticles within hollow zirconia[41], hollow silica[42] and tin oxide shells[43]. Our present design of Pt@mSiO$_2$ core–shell nanoparticles enables the direct access of reactive molecules to the catalytically active core metals. In addition, the Pt cores within the silica layer can be encaged even after high-temperature treatments while the faceted nature of the particle is preserved, showing great promise for use in high-temperature catalytic reactions.

The catalytic activity of Pt@mSiO$_2$ nanoparticles was investigated for ethylene hydrogenation. The ethylene hydrogenation was carried out at 10 torr of ethylene, 100 torr of H_2, with the balance He (see Supplementary Information for experimental details). The Pt@mSiO$_2$ exhibited a turnover frequency (TOF) of 6.9 s^{-1} at 25 °C and an activation energy of 8.1 kcal mol^{-1}. The TOF and activation energy are similar to those of the Pt single crystal, colloidal-Pt-nanoparticle-loaded SBA-15 model catalysts and other supported catalysts (see Supplementary Information, Table S1). It is worth noting that the Pt@mSiO$_2$ nanoparticles exhibited an order of magnitude higher TOF than the Pt@CoO yolk–shell nanoparticles[38]. The higher activity of Pt@mSiO$_2$ is probably due to the more facile diffusion and transport of the reactants and products

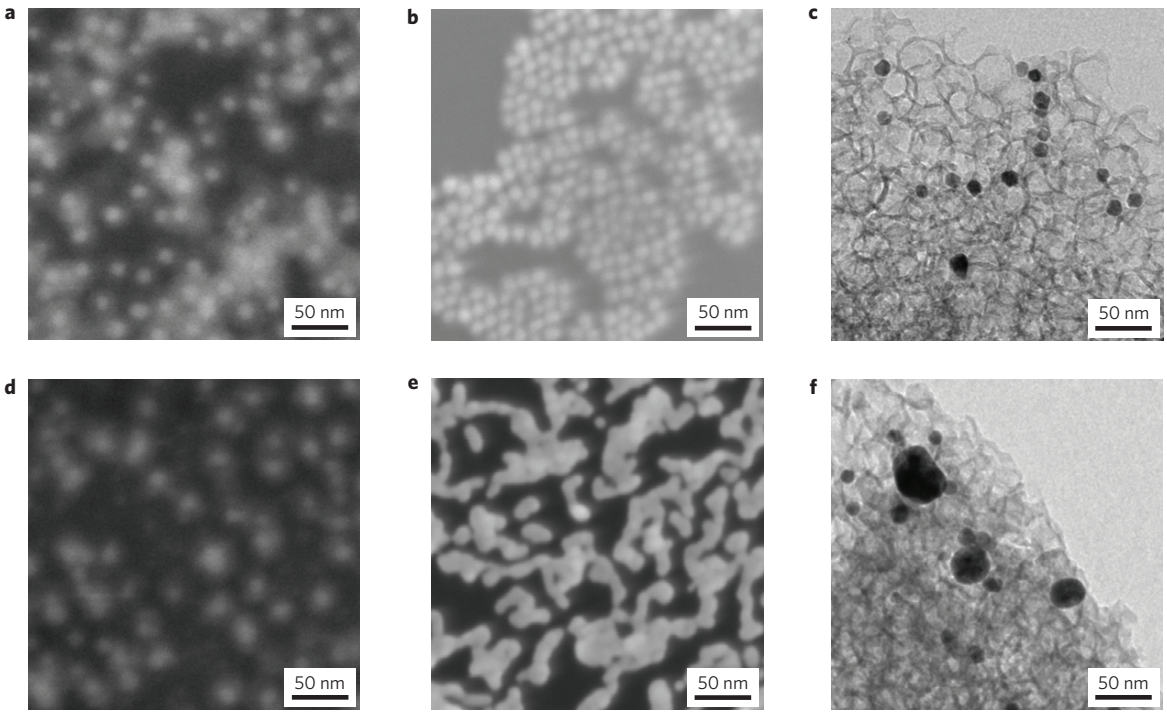

Figure 6 | Pt nanoparticle morphologies before and after CO oxidation. a–f, SEM images of core–shell Pt@mSiO$_2$ (**a**,**d**) and TTAB-capped Pt (**b**,**e**) nanoparticle arrays on 2D silicon wafer, and TEM images of TTAB-capped Pt nanoparticles dispersed on a 3D MCF mesoporous silica support (**c**,**f**) before (**a**–**c**) and after CO oxidation at 330 °C (**d**) and at 300 °C (**e**,**f**).

through the mesoporous silica shells in Pt@mSiO$_2$ than the CoO shell in Pt@CoO, where the grain boundaries in CoO were proposed as entry points for the molecules[38].

The high-temperature catalytic properties of Pt@mSiO$_2$ core–shell nanoparticles were explored by using CO oxidation as a model reaction. The catalytic oxidation of CO to CO$_2$ over platinum-group metals has been one of the most widely studied surface reactions owing to its significance for emission control and fuel cells[20–25]. In particular, from the mechanistic point of view, the CO oxidation reaction is intriguing as the reaction proceeds through different mechanisms below and above the ignition temperature. For the CO oxidation reaction, the Pt@mSiO$_2$ and Pt nanoparticles were deposited on a silicon wafer using the Langmuir–Blodgett technique. CO oxidation was carried out with excess O$_2$ (40 torr CO, 100 torr O$_2$, with the balance He) in the temperature range of 240–340 °C. Figure 5 shows the oxidation activity of the Pt@mSiO$_2$. Two distinct reaction regimes are observed as a function of temperature, which indicated an ignition temperature around 290–300 °C. For comparison, the TTAB-capped Pt nanoparticle catalyst on the silicon wafer was also tested for CO oxidation. The activity of the Pt@mSiO$_2$ catalyst was as high as that of TTAB-capped Pt nanoparticles, indicating that the silica shells in the Pt@mSiO$_2$ nanoparticles were porous enough to provide access to the Pt cores, which is consistent with our chemisorption and TEM studies. Figure 6 comparatively shows scanning electron microscope (SEM) and TEM images of TTAB-capped Pt nanoparticle arrays on the silicon wafer and Pt dispersed inside the mesopores of mesostructured cellular foam (MCF) silica (Pt/MCF), as well as the core–shell Pt@mSiO$_2$ before and after CO oxidation. The Pt@mSiO$_2$ catalyst after CO oxidation at 330 °C maintained the morphology of calcined particles (Fig. 6d). More importantly, the faceted and crystalline nature of the Pt cores in the Pt@mSiO$_2$ catalyst was preserved after the reaction, as shown in Supplementary Information, Fig. S4. However, the TTAB-capped Pt on silicon wafer (Fig. 6e) and Pt/MCF (Fig. 6f) exhibited severe aggregation of Pt particles after CO oxidation at 300 °C, which hampered the quantitative study of CO oxidation above the ignition temperature regime. The X-ray photoelectron spectroscopy (XPS) spectra of O1*s* peaks of Pt@mSiO$_2$ revealed that the Pt core was partially oxidized after CO oxidation (see Supplementary Information, Fig. S5).

The ignition temperature during CO oxidation over the Pt@mSiO$_2$ catalyst is 290–300 °C, which lies between that of Pt(100) (227 °C) and Pt(111) (347 °C) single crystals[25]. The Pt cores encaged in Pt@mSiO$_2$ nanoparticles are mostly composed of cubic and cuboctahedron shapes, exposing mostly (100) and (111) surfaces, which explains why the ignition temperature of the Pt@mSiO$_2$ nanoparticles is between those of Pt(100) and Pt(111) single crystals. The Pt@mSiO$_2$ nanoparticles exhibited lower activation energies (27.5 and 9.8 kcal mol^{-1} for below and above the ignition temperature, respectively) than Pt(111) single crystal (42 and 14 kcal mol^{-1}) (ref. 24) and (100) single crystal (32.9 kcal mol^{-1} for below ignition)[22]. For catalytic reactions on the surface to occur, the reacting molecules, reaction intermediates and products must alter their bond distances to enable rapid rearrangement. A relatively small number of bonds must also be broken and reformed as the catalytic chemistry occurs. The chemical bonds rearrange more easily on nanoparticles, where fewer atoms participate in the restructuring during catalytic turnover, than on single-crystal surfaces, and this phenomenon might be responsible for the origin of the lower activation energies.

In summary, the core–shell structured Pt@mSiO$_2$ nanoparticles were designed as high-temperature model catalysts. The Pt@mSiO$_2$ nanoparticles maintained their core–shell configurations up to 750 °C and exhibited high catalytic activity for ethylene hydrogenation and CO oxidation. The mesoporous silica coating chemistry on the nanoparticle surface is straightforward. Thus, the method can potentially be extended to other nanoparticle cores with different composition, size and shape and to other shell compositions. The CO oxidation study highlights the role of the thermally stable

inorganic silica shell in the Pt@mSiO$_2$ nanoparticles, which enables the study of catalytic reactions or surface phenomena taking place at high temperatures. Further application of core–shell catalysts to high-temperature reactions, such as partial oxidation and cracking of hydrocarbons and catalytic combustion, seems possible.

Methods

Synthesis of TTAB-capped Pt and Pt@mSiO$_2$ core–shell nanoparticles. The synthesis of TTAB-capped Pt nanoparticles was carried out by following the reported method with a modification[30]. The detailed synthesis procedure for Pt nanoparticles is described in Supplementary Information. The Pt@mSiO$_2$ core–shell nanoparticles were prepared by polymerizing the silica layer around the surface of Pt nanoparticles using a sol–gel process[33–35,44–46]. The Pt nanoparticle colloid (4.5×10^{-5} mol) dispersed in 5 ml of deionized water was added to 35.5 ml of deionized water. A NaOH solution (1.0 ml of 0.05 M) was added to the aqueous Pt colloid solution with stirring to adjust the pH of the solution to around 10–11. To this basic solution, a controlled amount of 10 vol% TEOS diluted with methanol was added to initiate the silica polymerization. The as-synthesized Pt@SiO$_2$ was calcined at 350 °C or higher for 2 h in static air to remove TTAB surfactants to generate Pt@mSiO$_2$ particles. The 2D model catalyst systems were fabricated by depositing the colloidal Pt and Pt@SiO$_2$ nanoparticles on a silicon wafer using the Langmuir–Blodgett technique (see Supplementary Information). MCF mesoporous silica with large mesopores, around 30 nm, was synthesized following the method in the literature[47] and TTAB-capped Pt nanoparticles were incorporated inside the pores of the MCF silica by capillary inclusion[48] to produce the 3D model catalyst.

Characterization. The particle size and shape were analysed with TEM images using a Philips/FEI Tecnai 12 microscope operating at 100 kV and an FEI Tecnai G^2 S-Twin electron microscope operating at 200 kV. XRD patterns were measured on a Bruker D8 GADDS diffractometer using Co Kα radiation (1.79 Å). Nitrogen physisorption experiments were carried out using a Quantachrome Autosorb-1 analyser at −196 °C. Before the measurement, degassing was conducted at 200 °C for 12 h to remove possible moisture. Hydrogen chemisorption was also carried out with a Quantachrome Autosorb-1 at 30 °C. Before the chemisorptions, the sample was heated to 300 °C for 1 h under H_2 and evacuated at 310 °C for 1.5 h, then cooled down to room temperature. The morphology and chemical composition of the 2D Langmuir–Blodgett films were characterized with a SEM and XPS, respectively. SEM images were taken on a Zeiss Gemini Ultra-55 with a beam energy of 5 kV. XPS spectra were taken on a 15 kV, 350 watt PHI 5400 ESCA/XPS system equipped with an Al anode X-ray source.

CO oxidation measurements. CO oxidation studies were carried out in an ultrahigh-vacuum chamber with a base pressure of 5.0×10^{-8} torr (ref. 19). The reactions were carried out under excess O_2 conditions: 40 torr CO, 100 torr O_2 and 620 torr He. The gases were circulated through the reaction line by a metal-bellows recirculation pump at a rate of 2 l min^{-1}. The volume of the reaction loop is 1.0 l. An HP Series II gas chromatograph equipped with a thermal conductivity detector and a 15′ long, 1/8″ outer diameter stainless-steel 60/80 mesh size Carboxen-1000 (Supelco) column was used to separate the products for analysis. The measured reaction rates are reported as TOFs and are measured in units of product molecules of CO_2 produced per metal surface site per second of reaction time. The number of metal sites is calculated by geometrical considerations based on SEM measurements of the surface area of a nanoparticle array.

Received 22 July 2008; accepted 15 October 2008; published online 23 November 2008

References

1. Bell, A. T. The impact of nanoscience on heterogeneous catalysis. *Science* **299**, 1688–1691 (2003).
2. Schlögl, R. & Abd Hamid, S. B. Nanocatalysis: mature science revisited or something really new? *Angew. Chem. Int. Ed.* **43**, 1628–1637 (2004).
3. Somorjai, G. A., Contreras, A. M., Montano, M. & Rioux, R. M. Clusters, surfaces, and catalysis. *Proc. Natl Acad. Sci. USA* **103**, 10577–10583 (2006).
4. Thomas, J. M. Heterogeneous catalysis: Enigmas, illusions, challenges, realities, and emergent strategies of design. *J. Chem. Phys.* **128**, 182502 (2008).
5. Somorjai, G. A. *Introduction to Surface Chemistry and Catalysis* (Wiley, 1994).
6. Over, H. *et al.* Atomic-scale structure and catalytic reactivity of the RuO_2(110) surface. *Science* **287**, 1474–1476 (2000).
7. Greeley, J. & Mavrikakis, M. Alloy catalysts designed from first principles. *Nature Mater.* **3**, 810–815 (2004).
8. Stamenkovic, V. R. *et al.* Improved oxygen reduction activity on Pt_3Ni(111) via increased surface site availability. *Science* **315**, 493–497 (2007).
9. Roucoux, A., Schulz, J. & Patin, H. Reduced transition metal colloids: A novel family of reusable catalysts? *Chem. Rev.* **102**, 3757–3778 (2002).
10. Park, J., Joo, J., Kwon, S. G., Jang, Y. & Hyeon, T. Synthesis of monodisperse spherical nanocrystals. *Angew. Chem. Int. Ed.* **46**, 4630–4660 (2007).
11. Tao, A. R., Habas, S. & Yang, P. Shape control of colloidal metal nanocrystals. *Small* **4**, 310–325 (2008).
12. Ahmadi, T. S., Wang, Z. L., Green, T. C., Henglein, A. & El-Sayed, M. A. Shape-controlled synthesis of colloidal platinum nanoparticles. *Science* **272**, 1924–1926 (1996).
13. Sun, Y. & Xia, Y. Shape-controlled synthesis of gold and silver nanoparticles. *Science* **298**, 2176–2179 (2002).
14. Song, H. *et al.* Hydrothermal growth of mesoporous SBA-15 silica in the presence of PVP-stabilized Pt nanoparticles: Synthesis, characterization, and catalytic properties. *J. Am. Chem. Soc.* **128**, 3027–3037 (2006).
15. Narayanan, R. & El-Sayed, M. A. Shape-dependent catalytic activity of platinum nanoparticles in colloidal solution. *Nano Lett.* **4**, 1343–1348 (2004).
16. Tian, N., Zou, Z.-Y., Sun, S.-G., Ding, Y. & Wang, Z. L. Synthesis of tetrahexahedral platinum nanocrystals with high-index facets and high electro-oxidation activity. *Science* **316**, 732–735 (2007).
17. Bratlie, K. M., Lee, H., Komvopoulos, K., Yang, P. & Somorjai, G. A. Platinum nanoparticle shape effects on benzene hydrogenation selectivity. *Nano Lett.* **7**, 3097–3101 (2007).
18. Alayoglu, S., Nilekar, A. U., Mavrikakis, M. & Eichhorn, B. Ru–Pt core–shell nanoparticles for preferential oxidation of carbon monoxide in hydrogen. *Nature Mater.* **7**, 333–338 (2008).
19. Park, J. Y., Zhang, Y., Grass, M., Zhang, T. & Somorjai, G. A. Tuning of catalytic CO oxidation by changing composition of Rh–Pt bimetallic nanoparticles. *Nano Lett.* **8**, 673–677 (2008).
20. Langmuir, I. The mechanism of the catalytic action of platinum in the reactions $2CO + O_2 = 2CO_2$ and $2H_2 + O_2 = 2H_2O$. *Trans. Faraday Soc.* **17**, 621–654 (1922).
21. Campbell, C. T., Ertl, G., Kuipers, H. & Segner, J. A molecular beam study of the catalytic oxidation of CO on a Pt(111) surface. *J. Chem. Phys.* **73**, 5862–5873 (1980).
22. Berlowitz, P. J., Peden, C. H. F. & Goodman, D.W. Kinetics of CO oxidation on single-crystal Pd, Pt, and Ir. *J. Phys. Chem.* **92**, 5213–5221 (1988).
23. Chen, M. S. *et al.* Highly active surfaces for CO oxidation on Rh, Pd, and Pt. *Surf. Sci.* **601**, 5326–5331 (2007).
24. Su, X., Cremer, P. S., Shen, Y. R. & Somorjai, G. A. High-pressure CO oxidation on Pt(111) monitored with infrared-visible sum frequency generation (SFG). *J. Am. Chem. Soc.* **119**, 3994–4000 (1997).
25. McCrea, K. R., Parker, J. S. & Somorjai, G. A. The role of carbon deposition from CO dissociation on platinum crystal surfaces during catalytic CO oxidation: Effects on turnover rate, ignition temperature, and vibrational spectra. *J. Phys. Chem.* **106**, 10854–10863 (2002).
26. Zaera, F. The surface chemistry of hydrocarbon partial oxidation catalysis. *Catal. Today* **81**, 149–157 (2003).
27. Huber, G. W. & Corma, A. Synergies between bio- and oil refineries for the production of fuels from biomass. *Angew. Chem. Int. Ed.* **46**, 7184–7201 (2007).
28. Ciuparu, D., Lyubovsky, M. R., Altman, E., Pfefferle, L. D. & Datye, A. Catalytic combustion of methane over palladium-based catalysts. *Catal. Rev.* **44**, 593–649 (2002).
29. Somorjai, G. A. & Rioux, R. M. High technology catalysts towards 100% selectivity. Fabrication, characterization and reaction studies. *Catal. Today* **100**, 201–215 (2005).
30. Lee, H. *et al.* Morphological control of catalytically active platinum nanocrystals. *Angew. Chem. Int. Ed.* **45**, 7824–7828 (2006).
31. Kresge, C. T., Leonowicz, M. E., Roth, W. J., Vartuli, J. C. & Beck, J. S. Ordered mesoporous molecular sieves synthesized by a liquid-crystal mechanism. *Nature* **359**, 710–712 (1992).
32. Corma, A. From microporous to mesoporous molecular sieve materials and their use in catalysis. *Chem. Rev.* **97**, 2373–2419 (1997).
33. Kim, M., Sohn, K., Na, H. B. & Hyeon, T. Synthesis of nanorattles composed of gold nanoparticles encapsulated in mesoporous carbon and polymer shells. *Nano Lett.* **2**, 1383–1387 (2002).
34. Nooney, R. I., Thirunavukkarasu, D., Chen, Y., Josephs, R. & Ostafin, A. E. Self-assembly of mesoporous nanoscale silica/gold composites. *Langmuir* **19**, 7628–7637 (2003).
35. Botella, P., Corma, A. & Navarro, M. T. Single gold nanoparticles encapsulated in monodispersed regular spheres of mesostructured silica produced by pseudomorphic transformation. *Chem. Mater.* **19**, 1979–1983 (2007).
36. van Hardeveld, R. & Hartog, F. The statistics of surface atoms and surface sites on metal crystals. *Surf. Sci.* **15**, 189–230 (1969).
37. Yu, R., Song, H., Zhang, X.-F. & Yang, P. Thermal wetting of platinum nanocrystals on silica surface. *J. Phys. Chem. B* **109**, 6940–6943 (2005).
38. Yin, Y. *et al.* Formation of hollow nanocrystals through nanoscale Kirkendall effect. *Science* **304**, 711–714 (2004).

39. Lin, K.-J., Chen, L.-J., Prasad, M. R. & Cheng, C.-Y. Core–shell synthesis of a novel, spherical, mesoporous silica/platinum nanocomposite: Pt/PVP@MCM-41. *Adv. Mater.* **16**, 1845–1849 (2004).
40. Ikeda, S. *et al.* Ligand-free platinum nanoparticles encapsulated in a hollow porous carbon shell as a highly active heterogeneous hydrogenation catalyst. *Angew. Chem. Int. Ed.* **45**, 7063–7066 (2006).
41. Arnal, P. M., Comotti, M. & Schüth, F. High-temperature-stable catalysts by hollow sphere encapsulation. *Angew. Chem. Int. Ed.* **45**, 8224–8227 (2006).
42. Lee, J., Park, J. C. & Song, H. A nanoreactor framework of a Au@SiO_2 yolk/shell structure for catalytic reduction of *p*-nitrophenol. *Adv. Mater.* **20**, 1523–1528 (2008).
43. Yu, K., Wu, Z., Zhao, Q., Li, B. & Xie, Y. High-temperature-stable Au@SnO_2 core/shell supported catalyst for CO oxidation. *J. Phys. Chem. C* **112**, 2244–2247 (2008).
44. Liz-Marzán, L. M., Giersig, M. & Mulvaney, P. Synthesis of nanosized gold-silica core–shell particles. *Langmuir* **12**, 4329–4335 (1996).
45. Lu, Y., Yin, Y., Li, Z.-Y. & Xia, Y. Synthesis and self-assembly of Au@SiO_2 core–shell colloids. *Nano Lett.* **2**, 785–788 (2002).
46. Gorelikov, I. & Matsuura, N. Single-step coating of mesoporous silica on cetyltrimethyl ammonium bromide-capped nanoparticles. *Nano Lett.* **8**, 369–373 (2008).
47. Schmidt-Winkel, P. *et al.* Microemulsion templating of siliceous mesostructured cellular foams with well-defined ultralarge mesopores. *Chem. Mater.* **12**, 686–696 (2000).
48. Rioux, R. M., Song, H., Hoefelmeyer, J. D., Yang, P. & Somorjai, G. A. High-surface-area catalyst design: Synthesis, characterization, and reaction studies of platinum nanoparticles in mesoporous SBA-15 silica. *J. Phys. Chem. B* **109**, 2192–2202 (2005).

Acknowledgements

This work was supported by the Director, Office of Science, Office of Basic Energy Sciences, Division of Chemical Sciences, Geological and Biosciences and Division of Materials Sciences and Engineering of the U.S. Department of Energy under contract No. DE-AC02-05CH11231. We thank A. P. Alivisatos and his group for the use of TEM and XRD equipment. We also thank J. N. Kuhn, Y.-w. Jun and J. Park for helpful comments and S. M. Ko for illustrations in Fig. 1.

Author contributions

G.A.S., P.Y., S.H.J. and J.Y.P. designed the research. S.H.J, C.-K.T. and Y.Y. carried out the synthesis and characterizations of nanoparticles. J.Y.P. and S.H.J. carried out catalysis experiments. S.H.J., J.Y.P., P.Y. and G.A.S. wrote the paper.

Additional information

Supplementary Information accompanies this paper on www.nature.com/naturematerials. Reprints and permissions information is available online at http://npg.nature.com/reprintsandpermissions. Correspondence and requests for materials should be addressed to G.A.S.

Supplementary Information for

Thermally Stable Pt-Mesoporous Silica Core-Shell Nanocatalysts for High Temperature Reactions

Sang Hoon Joo, Jeong Young Park, Chia-Kuang Tsung, Yusuke Yamada, Peidong Yang and Gabor A. Somorjai*

Department of Chemistry, University of California, Berkeley, and Chemical Sciences and Materials Sciences Divisions, Lawrence Berkeley National Laboratory, Berkeley, California 94720, USA.

** e-mail: somorjai@berkeley.edu*

Experimental Details

1. Synthesis of TTAB-capped Pt nanoparticles

For the synthesis of Pt nanoparticles, 5 mL of aqueous 10 mM K_2PtCl_4 (Aldrich, 99.9%) and 12.5 mL of 400 mM TTAB (Aldrich, 99%) were mixed with 29.5 mL of deionized water (DI) in a 100-mL round bottom flask at room temperature. The mixture was stirred at room temperature for 10 min and was heated at 50 ^oC for 10 min. To the clear solution, 3 mL of 500 mM ice-cooled $NaBH_4$ (Aldrich, 98%) solution was injected through the septum using a syringe. The gas evolved inside the flask was released by inserting a needle through the septum for 20 min. The needle was then removed and the solution was kept at 50 ^oC for 15 h. The product was centrifuged at 3000 rpm for 30 min. The supernatant solution was separated and centrifuged again at 14000 rpm for 15 min, twice. The Pt nanoparticle colloids were collected and re-dispersed in 5 mL of deionized water by sonication for further use.

2. Fabrication of Langmuir-Blodgett films of Pt and Pt@SiO_2 nanoparticles

Colloidal Pt or Pt@SiO_2 nanoparticle solutions were dispersed on the surface of DI subphase on a LB trough (type 611, NIMA Technology) at room temperature. The surface pressure was monitored with a Wilhelmy plate and adjusted to zero before spreading the nanoparticles. The resulting surface layer was compressed by a mobile barrier at a rate of 20 $cm^2\,min^{-1}$. The nanoparticles were deposited by lifting up the silicon substrates (which had been immersed in water subphase before the nanoparticles were dispersed) at a surface pressure of ~12 $mN\,m^{-1}$.

3. Measurement of ethylene hydrogenation

The ethylene hydrogenation was conducted in a plug flow reactor made of Pyrex. Reactants and products were detected by gas chromatography (Hewlett-Packard 5890 Series II). Rate measurement for ethylene hydrogenation was conducted at differential conditions (all conversions < 10%).

Catalyst	E_a (kcal mol^{-1})	TOF (s^{-1}) [a]	Reference
Pt(111)	10.8	9.3	(1)
Pt nanoparticle array	10.2	14.3	(2)
0.5 % Pt/SiO_2	8.9	17.5	(3)
0.04 % Pt/SiO_2	8.6	4.4	(4)
~ 1 % Pt/SBA-15 by capillary inclusion	7	~ 0.7	(5)
~ 1 % Pt/SBA-15 by nanoencapsulation	10~12	~ 3.5	(6)
14% Pt@CoO	5.0	0.29	(7)
$Pt@mSiO_2$	8.1	6.9	This Work

[a] Reaction conditions were 10 Torr C_2H_4, 100 Torr H_2, and 298 K.

References for Table S1

(1) Zaera, F. & Somorjai, G. A. *J. Am. Chem. Soc.* **106**, 2288–2293 (1984).

(2) Grunes, J., Zhu, J., Anderson, E. A. & Somorjai, G. A. *J. Phys. Chem. B* **106**, 11463–11468 (2002).

(3) Schlatter, J. C. & Boudart, M. *J. Catal.* **24**, 482–492 (1972).

(4) Cortright, R. D., Goddard, S. A., Rekoske, J. E. & Dumesic, J. A. *J. Catal.* **127**, 342–353 (1991)

(5) Rioux, R. M., Song, H., Hoefelmeyer, J. D., Yang, P. & Somorjai, G. A. *J. Phys. Chem. B* **109,** 2192–2202 (2005).

(6) Song, H. *et al*., *J. Am. Chem. Soc.* **128**, 3027–3037 (2006).

(7) Somorjai, G. A. & Rioux, R. M. *Catal. Today* **100**, 201–215 (2005).

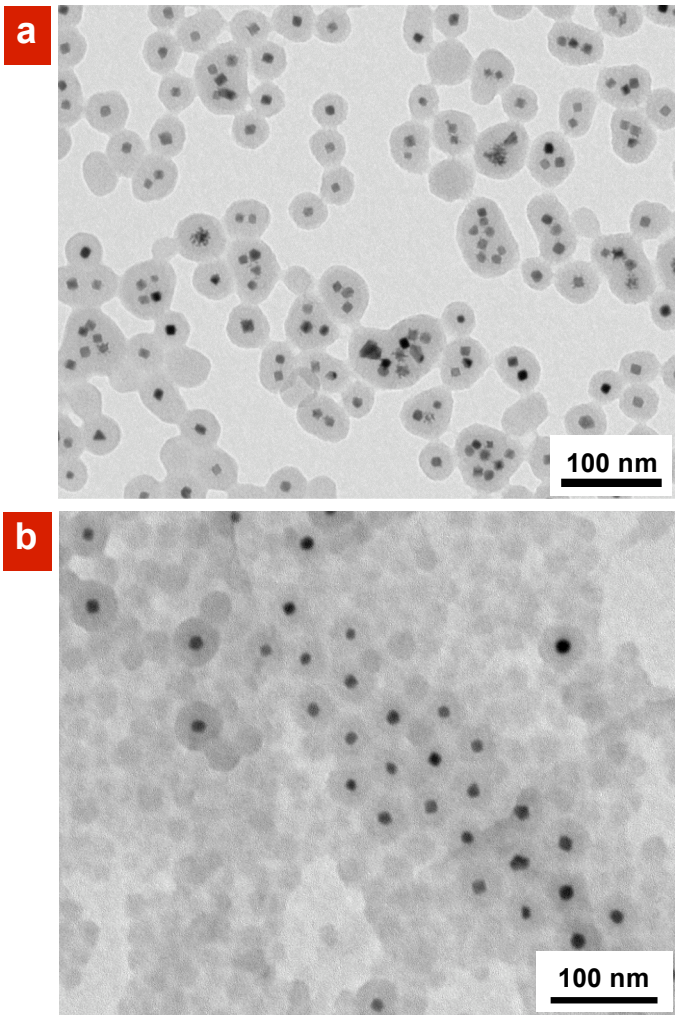

Figure S1. Pt@SiO_2 core-shell nanoparticles synthesized under (a) lower and (b) higher concentrations of TEOS, compared to the Pt@SiO_2 nanoparticles synthesized under the optimum TEOS concentration where each Pt particle is encaged within a silica shell.

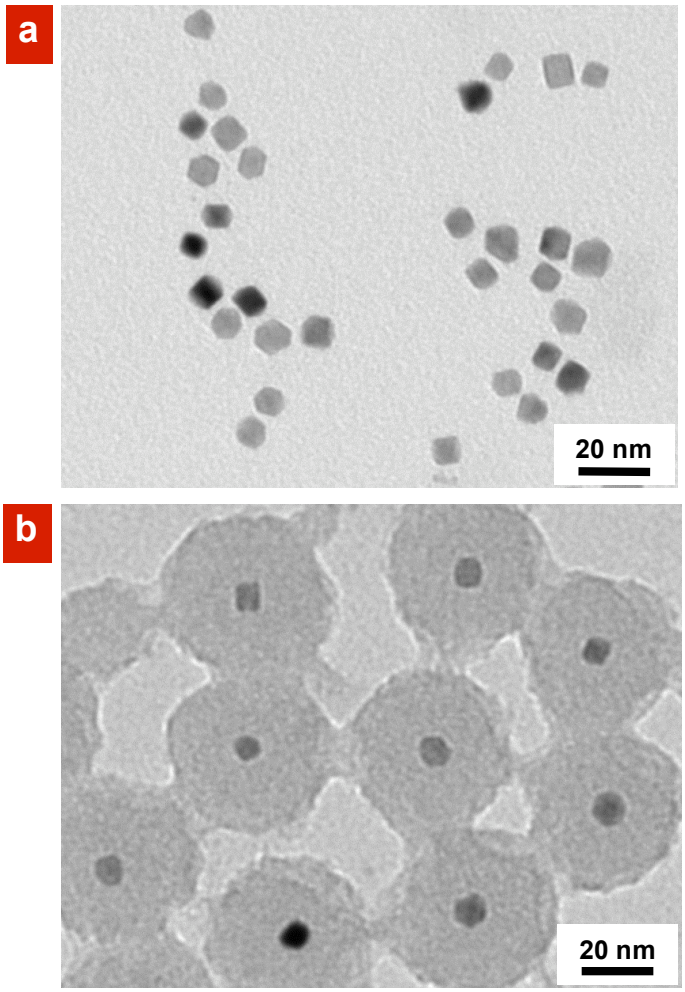

Figure S2. TEM images of (a) 8.5 nm Pt and (b) corresponding Pt@SiO_2 core-shell nanoparticles. The shell thickness of these nanoparticles was found to be ~ 18 nm, similar to that of core-shell nanoparticles with 14 nm Pt core.

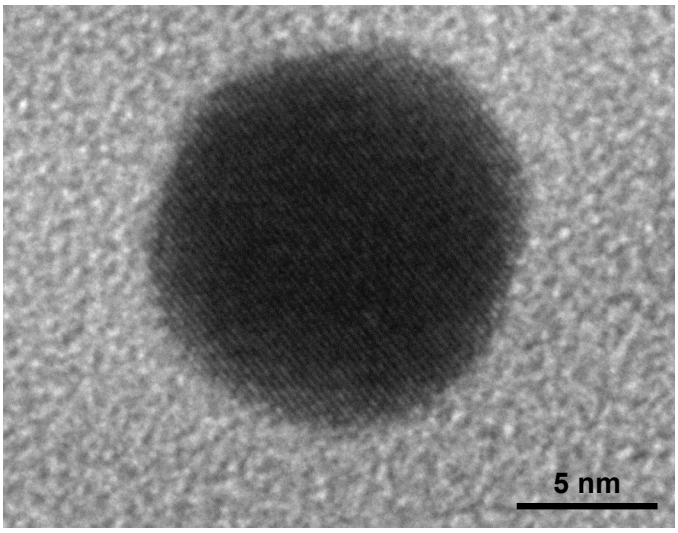

Figure S3. High resolution TEM image Pt core in Pt@mSiO_2 core-shell nanoparticle after calcination at 350 ^{o}C.

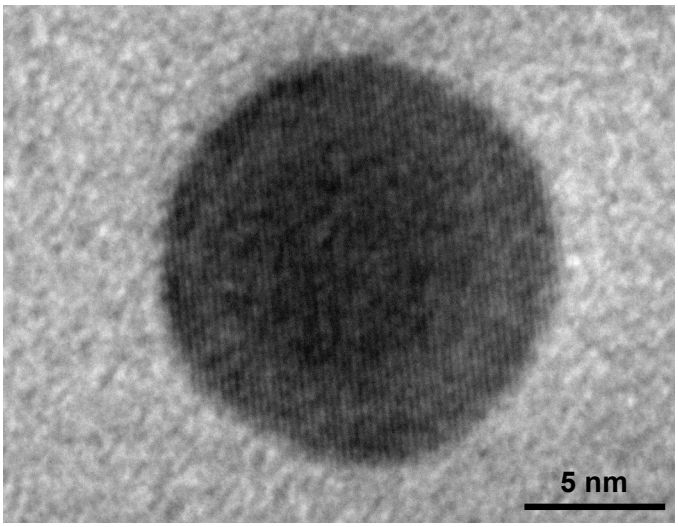

Figure S4. High resolution TEM image Pt core in Pt@mSiO_2 core-shell nanoparticle after calcination and subsequent CO oxidation.

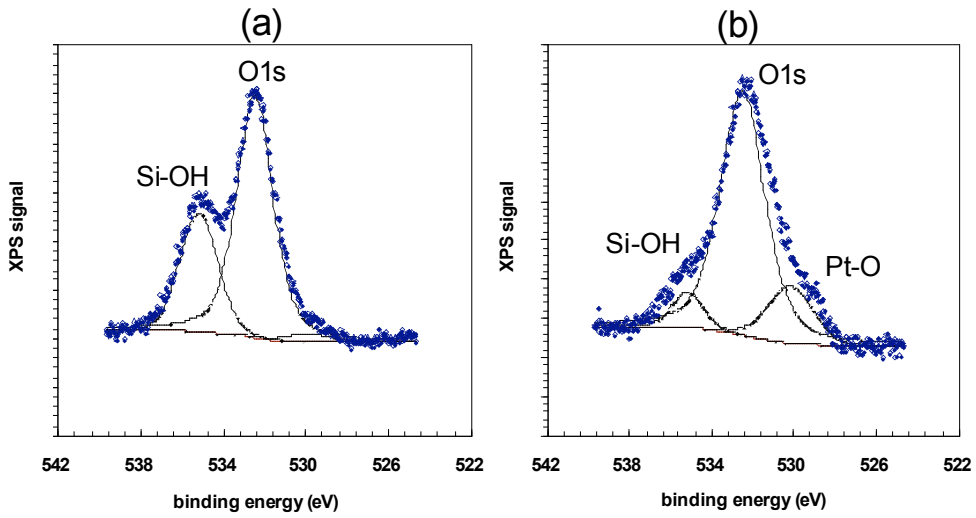

Figure S5. XPS plots of Pt@SiO_2 core-shell nanoparticles (a) before and (b) after calcination and CO oxidation. The Pt@SiO_2 nanoparticles were deposited on a silicon wafer using the Langmuir-Blodgett (LB) technique. The maximum temperature for CO oxidation was 340 °C. The binding energy for XPS measurements was calibrated with the C1s peak (285 eV). O1s is presumably attributed to the SiO_2 oxygen. The as-synthesized sample exhibits two peaks of hydroxides and atomic oxygen. After calcination, the hydroxide peak decreased and a small peak, that is attributed to Pt-O, appeared, suggesting that Pt core is partially oxidized during the catalytic reactions.